16th World Conference on Earthquake Engineering, 16WCEE 2017

Santiago Chile, January 9th to 13th 2017

Paper N° 2409

Registration Code: S-P1464780593

HIGH FIDELITY MONOTONIC AND CYCLIC SIMULATION OF A WOOD-SHEATHED COLD-FORMED STEEL FRAMED FLOOR DIAPHRAGM

A. Chatterjee[(1)], C.A. Rogers[(2)], C. D. Moen[(3)]

[(1)] *Graduate Research Assistant, Virginia Tech, aritrac1@vt.edu*
[(2)] *Associate Professor, McGill University, colin.rogers@mcgill.ca*
[(3)] *Associate Professor, Virginia Tech, cmoen@vt.edu*

Abstract

Non-linear finite-element models of monotonic and reversed cyclic wood sheathed cold-formed steel (CFS) framed diaphragm tests recently conducted at McGill University are developed using the commercial finite element software ABAQUS. Cantilever-type monotonic and reversed cyclic tests to failure were conducted on 3.5 m x 6.1 m wood sheathed cold-formed steel framed diaphragm specimens. The diaphragm construction details matched those used for previous full-scale shake table experiments performed on a two-story building under the CFS-NEES project. Oriented strand board (OSB) sheathing, cold-formed steel joists, tracks, blocking and clip angles are modeled as elastic shell finite elements. Sheathing-to-steel screw connections are modeled as non-linear shear spring elements that were characterized using single fastener tests. The spring models are multi-linear with two ascending branches and two descending branches. For the reversed cyclic analysis, the fasteners are modeled with recently developed User Element Library that can capture unloading-reloading response under reversing loads. Contact is modeled between the OSB panels using a combination of bearing and frictional springs. The analysis results are compared to the laboratory tests for initial stiffness, peak load, ductility and energy dissipation. Force distributions in individual fastener components that are critical to system behavior are studied. This work gives insight into the seismic response and flow of forces in floor diaphragms and verifies a cyclic modeling protocol for cold-formed steel framed structural systems.

Keywords: Cold-formed steel; Diaphragms; Finite-element simulation; Cyclic experiments; Connections

1. Introduction

Non-linear finite-element models of monotonic and reversed cyclic wood sheathed cold-formed steel (CFS) framed diaphragm tests recently conducted at McGill University [1, 2] are developed using the commercial finite element software ABAQUS. This research focuses on the seismic behavior of diaphragms sheathed with oriented strand-board (OSB) panels, typically 1220mm X 2440 mm, attached to cold-formed steel (CFS) framing members with minimum #8 sized screw fasteners (4.1 mm diameter). This construction style is typical in light-framed steel buildings.

The limited experimental data available on wood-sheathed cold-formed steel diaphragms highlight the importance of the screw fastener connections [3]. Previous experiments were performed on a 3650 mm by 7300 mm floor subsystem by the National Association of Home Builders (NAHB) [3]. Lateral loads were applied along one edge while the other edges running parallel to the direction of loading were held fixed to represent the stiff shear walls. Diaphragm load-deformation softening resulted from screws tilting and tearing through plywood sheets that translate and rotate as rectangular rigid bodies.

The McGill tests and simulations discussed in this paper supplement full-scale light-framed building tests recently performed on a prototype two story building (NEES building) at the Johns Hopkins University [4]. The experiments applied scaled ground motions up to 100% the design basis earthquake (DBE, Canoga Park) and maximum considered earthquake (MCE, Rinaldi), with and without non-structural components. The McGill tests characterize the diaphragm force-deformation response, ductility and cyclic energy dissipation as it is loaded in shear along one edge with the other held fixed. Similar to previous experimental results and design code predictions, the tests indicate that the diaphragm response is governed by tilting and bearing behavior of screw-fastened connections between the OSB panels and the underlying steel framing. These connections are characterized as multi-linear backbone with unloading-reloading response parameters obtained from cyclic single connection experiments conducted at Virginia Tech.

The connection monotonic and cyclic response parameters are implemented in this paper with high-fidelity computational models simulating the McGill diaphragm experiments performed with the general-purpose finite element software ABAQUS [5]. The models include custom user-defined elements for the screw-fastened connections that update their orientations during the analysis and include cyclic unloading-reloading response [6]. The simulation results are compared with the tested diaphragm response to validate monotonic pushover and cyclic finite-element modeling protocols for cold-formed steel framing. The calibrated modeling protocol provides the capability to explore other diaphragm configurations, sizes, aspect ratios, and component properties (sheathing, joist and fastener details) since repeating experiments of this size is difficult and time-consuming.

2. Wood-sheathed cold-formed steel framing tests at McGill

2.1 Test matrix

Two different test configurations [1, 2] corresponding to the NEES building details were considered in the experimental program, one matching the NEES roof and the other corresponding to the NEES second-floor diaphragm (Table 1). Since the roof configuration showed failure due to panel uplift, a blocked diaphragm configuration, characterized by supporting cold-formed steel framing underlying all panel edges, was also tested. An additional floor diaphragm configuration using #12 (5.5 mm) fasteners was built since this is customary in cold-formed steel construction for the sheathing and joist thicknesses considered (Table 2), although the baseline NEES floor diaphragm used #10 (4.8 mm) fasteners.

Table 1 -- Test matrix for diaphragm experiments conducted at McGill

Test configuration	NEES roof	NEES roof	NEES second floor #10 fasteners	NEES second floor #10 fasteners	NEES roof blocked	NEES roof blocked	NEES second floor #12 fasteners	NEES second floor #12 fasteners
Type of test	Monotonic	Cyclic	Monotonic	Cyclic	Monotonic	Cyclic	Monotonic	Cyclic
Number of tests	1	1	1	1	1	1	1	1

Figure 1 -- Specimen description showing arrangement of sheathing, floor joists, rim tracks and blocking

2.2 Specimen details

The overall specimen dimension was 6100 mm wide by 3660 mm deep with three rows of 1220 mm X 2440 mm OSB panels arranged in a staggered configuration as shown in Figure 1.

The material and cross-sectional parameters for the diaphragm components vary from the floor to the roof configuration and are described in Table 2. The sectional notations, described in [7], are explained here for convenience. For joist, track and blocking Cee cross-section notations, the first number preceding the letter is the out-to-out web depth in hundredths of an inch, the letter indicates the section type (S stands for a stud section with flanges stiffened with lips whereas T indicates an unlipped track section), the number following the letter preceding the hyphen indicates the flange width in hundredths of an inch, and the final number subsequent to the hyphen is the nominal sectional thickness in thousands of an inch. For example, joist sections for the floor specimen are designated as1200S250-97, indicating lipped Cee sections where the 1200 means a 12 inch (305 mm) out-to-out web depth, 250 means a 2.50 inch (63.5 mm) out-to-out flange width, and 97 corresponds to a base metal thickness of 2.56 mm. The third number for the L-shaped clip angle sections designates the nominal specimen thickness in thousands of an inch, as does the second number for strap sections.

Table 2 -- Component cross-section details for floor and roof diaphragm test specimens

Component type	Section used in roof specimen	Section used in floor specimen
Joists	1200S200-54	120S250-97
Tracks	1200T200-68	1200T200-68
Joist-to-track clip angles	L 1.5 in. X 1.5 in. X 54	L 1.5 in. X 1.5 in. X 54
Blocking	1200S162-54	1200S200-54
Joist-to-blocking clip angles	L 1.5 in. X 4 in. X 54	L 1.5 in. X 4 in. X 54
Straps	1.5 in. X 54	1.5 in. X 54
OSB sheathing panels	24/16 rated, 8 ft. X 4 ft. X 7/16 in.	48/24 rated, 8 ft. X 4 ft. X 23/32 in.
Sheathing to steel fasteners	#8 flat head (4.1 mm diameter)	#10 flat head (4.8 mm diameter) or #12 flat head (5.5 mm)
Steel to steel fasteners	#10 hex head (4.8 mm diameter)	#10 hex head (4.8 mm diameter)

2.3 Loading and boundary conditions

The specimen was attached to the test frame along its longer edges via hot-rolled W sections, as shown in Figure 2. One of the two W sections was loaded with a 450KN actuator attached mid-way along its length, while the other was fixed in place. The W sections connected to the CFS ledger track via twelve pairs of bolts spaced at 610 mm along its length.

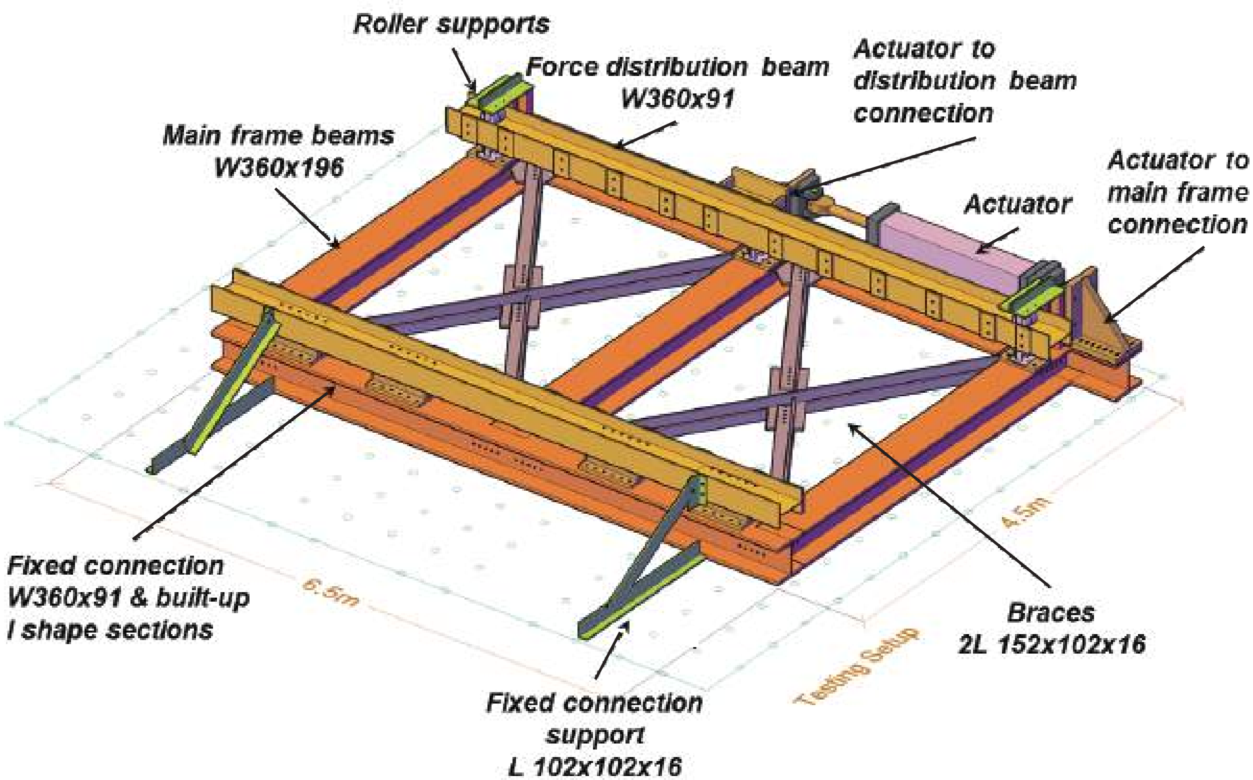

Figure 2 -- Testing frame showing supporting hot-rolled steel framing and actuator attachment points [1, 2]

2.4 Fastener connection properties

Sheathing to framing screw fasteners are characterized as quadri-linear springs according to recommendations given in [8] with unloading-reloading response described by the *Pinching4* model [9] used in the earthquake engineering simulation platform OPENSEES [10]. The connection backbones have an initial elastic branch, followed by strain hardening, softening and failing branches. The multi-linear backbone parameters, described in Figure 3, include the peak strength F_c, the cap deformation δ_c, yield strength and deformation F_y and δ_y, failure load F_r and deformation at failure δ_r, and initial, hardening, softening and residual stiffness K_e, K_s, K_c and K_r. The unloading-reloading response is characterized by forces and deformations at the onset and termination of unloading/reloading, expressed as a ratio of the maximum values of the deformation history using parameters *rDispP*, *rDispN*, *r ForceP*, *rForceN*, *uForceP* and *uForceN*. The parameters are estimated from cyclic fastener experiments conducted as per the protocol described in [11], followed by a least squared optimization on the backbones forces and hysteretic energy dissipated, according to recommendations given in [12]. The backbone and pinching parameters values are listed in Table 3 for the different connection combinations used in the diaphragms.

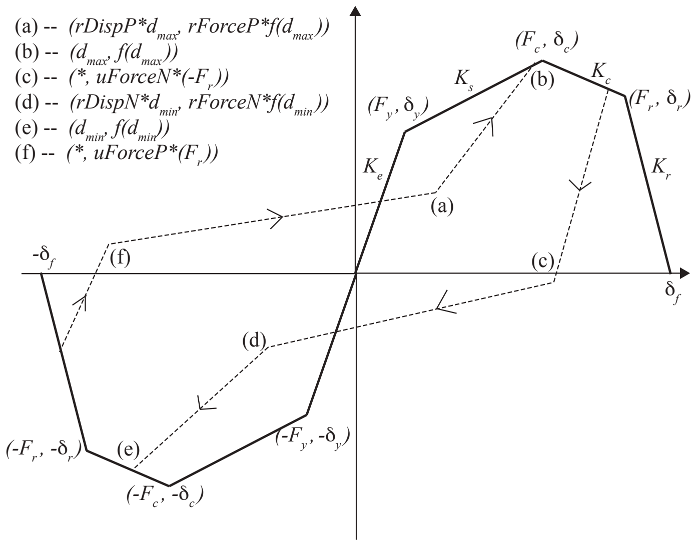

Figure 3 – Quadri-linear backbone parameters and pinching parameters used to characterize monotonic and cyclic fastened connection force-deformation response

Table 3 -- Backbone and pinching parameters for sheathing-to-steel screw-fastened connections

Component type	Fy [kN]	Fc [kN]	Fr [kN]	dy [mm]	dc [mm]	dr [mm]	df [mm]	rDispP	rForceP	rDispN	rForceN
Roof Sheathing to Field Joist #8 Fasteners	1.06	2.21	1.77	0.47	4.2	9.7	21	0.3141	0.0114	0.3909	0.0123
Roof Sheathing to Rim Track #8 Fasteners	1.38	2.17	1.60	0.80	6.1	8.5	13	0.4149	0.0113	0.4708	0.0107
Floor Sheathing to Field Joist #10 Fasteners	1.43	2.55	1.77	0.31	5.6	6.0	6.7	0.3096	0.0153	0.0040	0.0142
Floor Sheathing to Rim Track #10 Fasteners	1.20	2.55	2.50	0.18	5.7	6.0	7.3	0.3096	0.0153	0.0040	0.0142
Floor Sheathing to Field Joist #12 Fasteners	2.33	4.36	4.03	0.59	7.9	11	12	0.3410	0.0116	0.4779	0.0112
Floor Sheathing to Rim Track #12 Fasteners	2.10	4.37	4.09	0.72	8.3	11	12	0.3410	0.0116	0.4779	0.0112

Typical deformation cycles obtained experimentally are compared to the modeled cycles in Figure 4 for a representative connection experiment for each material combination tested. Cumulative hysteretic energy dissipated in the experiments are compared to the Pinching4 model energy dissipation in Figure 5.

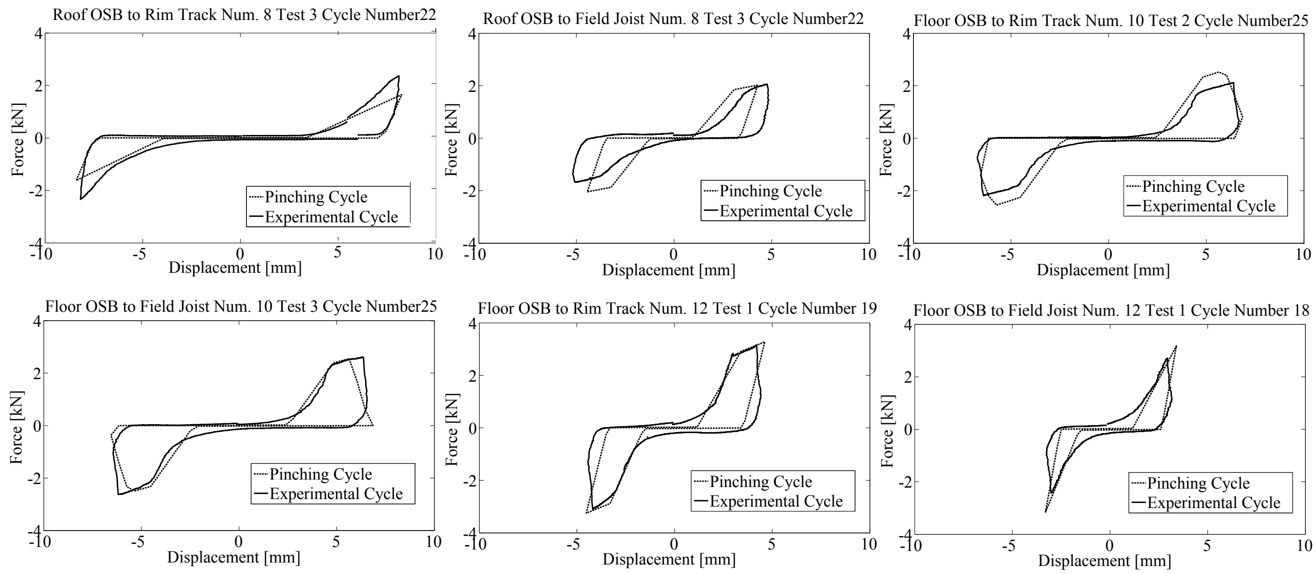

Figure 4 -- Representative comparisons between experimentally obtained cyclic force-deformation relationships and modeled connection pinching behavior

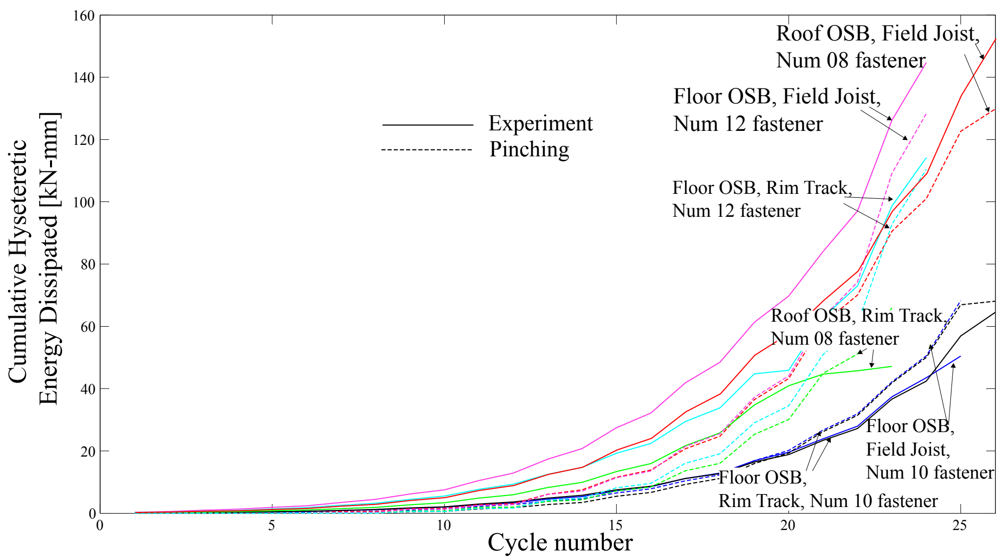

Figure 5 -- Cumulative hysteretic energies dissipated experimentally and in the pinching model for different connection specifications

2.5 Tested load-deformation response

The diaphragm tests indicated limited ductility with the dominant failure mode being sheathing-to-steel connection failure. For the roof diaphragm specimen, wood bearing followed by tear-out and pull-through of the screw connections were observed. Panel lift-off was also observed at interior locations on panels (not at panel-edges) where the panels were supported at 610 mm, which is the spacing between the joists. In the floor specimen, the higher sized (#10) screws failed mostly in shear and did not undergo significant tilting. Monotonic force-deformation responses are plotted in Figure 8, where they compared to the computationally obtained response, while cyclic responses are plotted in Figure 6.

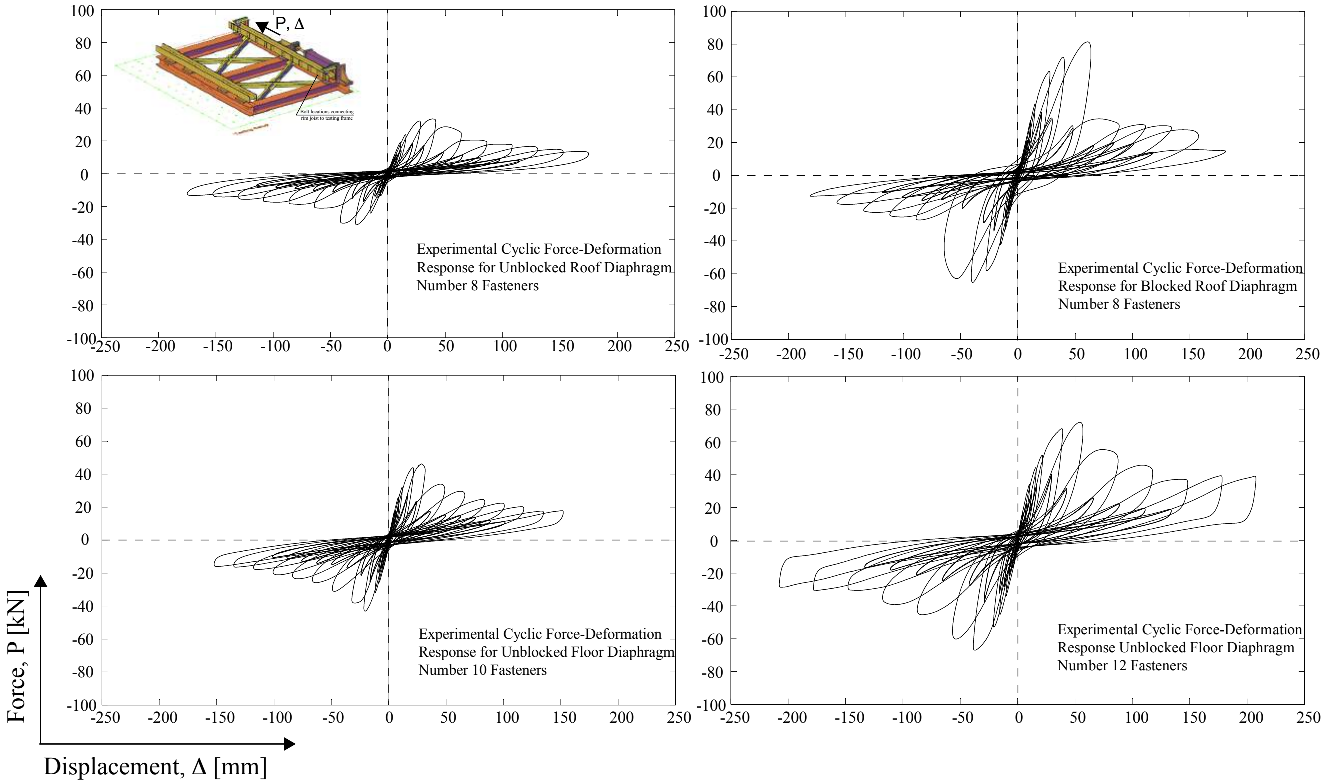

Figure 6 -- Experimentally obtained cyclic force-deformation responses for floor diaphragm [1, 2]

3. Simulations of McGill wood-sheathed cold-formed steel framing tests

3.1 Meshing and geometry

The finite-element modeling protocol was derived from recommendations provided in [13]. Cold-formed steel joists, rim tracks, wood panels, clip angles and blocking in the floor diaphragm are modeled in ABAQUS with four-node S4R thin shell elements. Element aspect ratios are approximately 1:1 and mesh size is typically 25.4 mm (Figure 7). The flange and web dimensions as well as fastener locations dictate local changes in mesh density [14].

3.2 Boundary conditions

The model boundary conditions were chosen to match the test setup. A displacement boundary condition was applied to the nodes connecting the rim track to the hot-rolled W section along one edge, with all other degrees of freedom restrained to account for the stiff restraint provided by the bolts. The other diaphragm edge that was held fixed during the tests was constrained in all six degrees of freedom at the bolt locations (Figure 7).

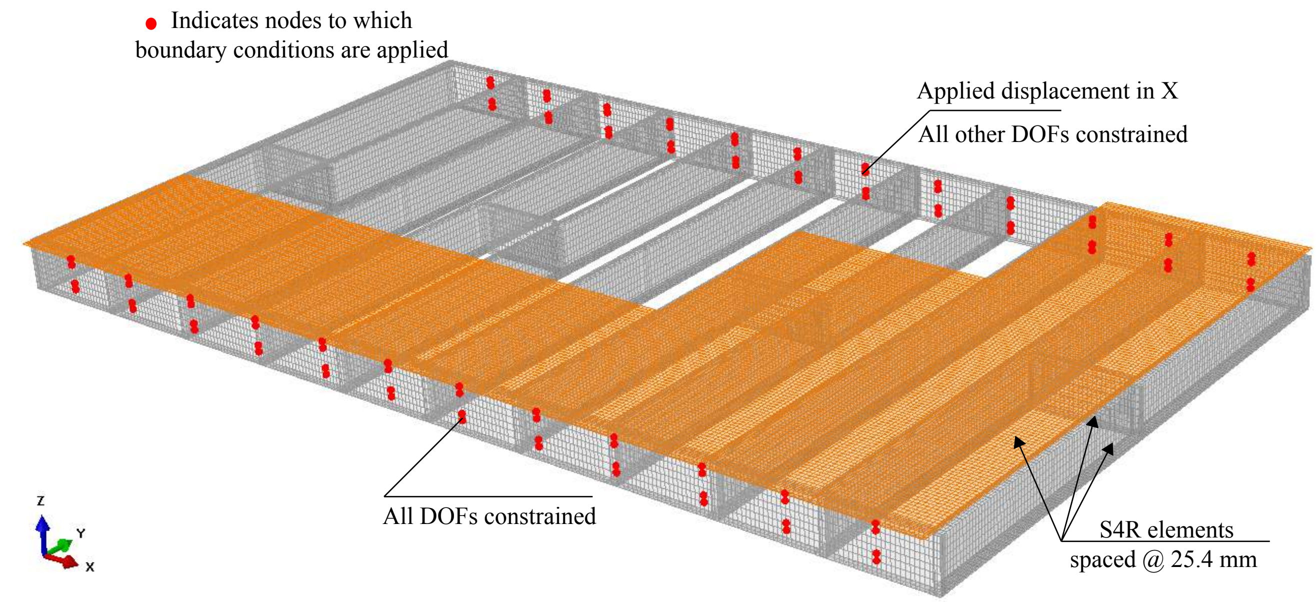

Figure 7 -- Mesh density and boundary conditions for finite-element model developed in ABAQUS

3.3 Cyclic fastener modeling

Sheathing to framing (field and rim joists or tracks) fasteners, spaced at 152 mm along panel edges and 305 mm in the field, are modeled as custom user elements (UEL option in ABAQUS) that were developed in [6]. These elements act as non-linear radial springs which update their orientations during the analysis, and capture unloading and reloading response under cyclic loads. Monotonic and cyclic backbones for these springs are defined as quadri-linear force-deformation relationships with a pinching behavior under cyclic loading as described in [9, 12]. The quadri-linear backbone and pinching parameters are listed in Table 3.

3.4 Modeling contact between sheathing panels

Three kinds of contact behavior are modeled between the sheathing panels – bearing, uplift and in-plane friction. Bearing is modeled by non-linear springs that have infinite stiffness in compression and zero stiffness in tension spaced at 76 mm along the panel edges that prevent the panels from penetrating into one another but allow separation [15].

Uplift was observed during the diaphragm experiments for the unblocked roof configuration but did not occur for the floor configuration due to the tongue-in-groove characteristics of the sheathing. As such, the floor diaphragm models included coupling in the direction of uplift (degree of freedom Z in Figure 7) between panel edges, but this was excluded in the roof diaphragm models.

Finally, both the roof and floor diaphragm experiments indicated partial in-plane friction between panel edges. Accordingly, the computational model response was found to be too stiff when perfect in-plane panel-to-panel coupling was modeled, and too flexible when it was completely excluded. Assuming that the normal force between the panels is proportional to the length in contact, partial friction was modeled using springs spaced at 76 mm. The force-deformation relationship of the frictional springs was non-linear and increased as a step function as the relative deformation exceeded zero (static friction). The spring force was capped at 0.07 kN for the roof diaphragm and 0.22 kN for the floor diaphragm, which is the panel-to-panel frictional force per 76 mm of panel contact.

The spring force is verified with the panel-to-panel sliding displacement using the assumed relationship $P_{friction}=P(\Delta_{max})*(\Delta_{max}-\Delta_{sliding})/\ \Delta_{max}$, where $P(\Delta_{max})$ is the diaphragm load at peak cyclic displacement (12 kN for #8 roof and 27 kN for #12 floor experiments), Δ_{max} is the maximum diaphragm displacement and $\Delta_{sliding}$ is the relative slip between panels. For the roof diaphragm, $\Delta_{sliding}$ approximately equals 0.6 Δ_{max}, while for the floor it is approximately 0.4 Δ_{max}, resulting in $P_{friction}$=5.08 kN in the roof and $P_{friction}$=16.4 kN in the floor for 6096 mm length of contact, or 0.06 kN and 0.20 kN respectively per 76 mm of contact.

3.5 Material constitutive laws

The steel elastic modulus is assumed as 200 GPa with a Poisson’s ratio of 0.30. The OSB is modeled as isotropic with an elastic modulus of 2.4 GPa and Poisson’s ratio of 0.30. This is based on shear modulus recommendations provided in the International Building Code Table 2305.2.2 [16] for rated OSB sheathing. Plasticity is modeled in the cold-formed steel joists and tracks by specifying plastic strains at post-yield stresses using recommendations provided in [17]. Initial geometric imperfections are not modeled since the slender elements (joists, tracks, panels) experience minimal compressive stresses and loading imperfections naturally present can trigger second order out-of-plane deformations.

3.6 Monotonic and cyclic loading

Loads are applied as a displacement boundary condition as explained in Figure 7. Static general analysis in ABAQUS is used throughout which employs the Newton-Raphson solution algorithm. For monotonic analyses, the initial displacement step is set at 1.3 mm with automatic time-stepping set to a maximum allowable increment size of 13mm. For cyclic analysis the initial as well as the maximum displacement increment is set at 0.25 times the amplitude at each cycle.

3.7 Simulated load-deformation response and failure modes

Experimental and computational load-deformation responses are plotted in Figure 8. The computational model matches the peak load for all three unblocked diaphragm configurations. For the floor diaphragm with #10 screw fasteners and roof diaphragm with #8 screw fasteners, the initial stiffness is over-predicted whereas the secant stiffness at failure is under-predicted, which possibly results from the large variability in connection backbone stiffnesses observed experimentally [11], or the assumed panel edge friction spring stiffness values.

As can be observed in Figure 8, the computational response matches the experimental plots quite well until peak capacity. The models face a convergence limit when the fasteners begin to fail. This limit is reached as soon as the second fastener reaches its peak load for the floor #10 configuration, whereas in the floor #12 configuration 20 fasteners surpass their ultimate capacity which creates the jagged shape of the overall response. On the other hand, the roof diaphragm configuration shows a gradual plateau in the load-deformation response after peak capacity is reached, and includes 51 fasteners exhibiting post-peak response. These features are attributed to the individual force-deformation relationships of the failing fasteners, which are plotted in Figure 9. The floor #10 connection backbones have the highest un-loading stiffness which leads to convergence difficulties, whereas the floor #12 and roof #8 connections have relatively flatter unloading branches, allowing the solution algorithm to capture a greater portion of the post-peak response.

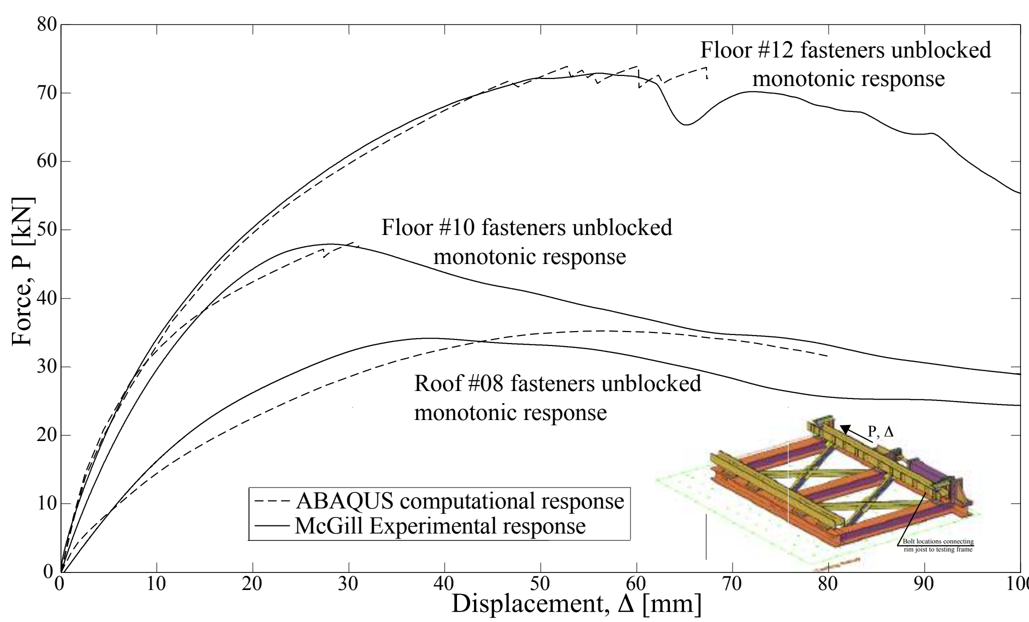

Figure 8 -- Computational and monotonic force-deformation response for unblocked floor and roof diaphragms

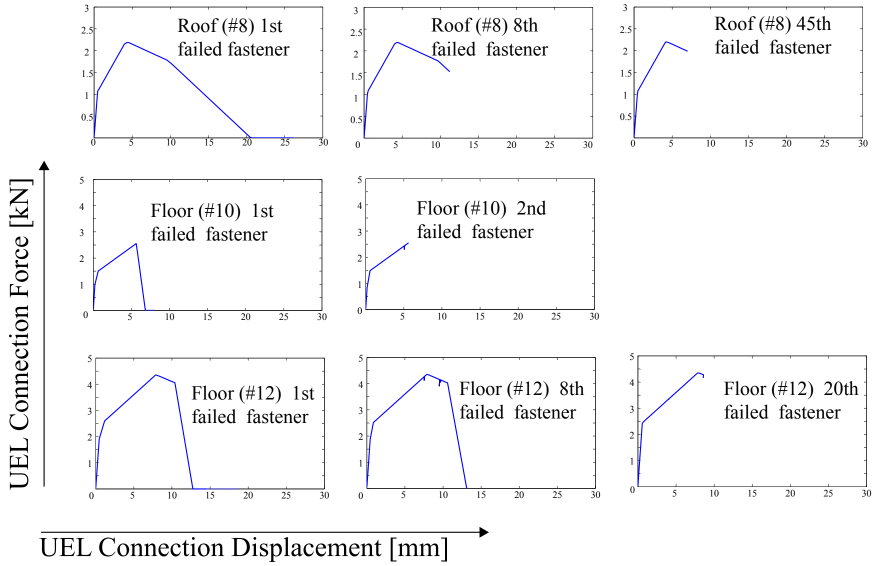

Figure 9 -- Failing fasteners load-deformation history indicating how the brittleness of the unloading leg affects convergence of the computational model

For all the configurations tested, failures were driven by the sheathing-to-steel screw fastened connection response. In the roof configuration, this included bearing on the wood followed by tear-out and fasteners pulling through the sheathing. Furthermore, the unblocked roof configuration exhibited panel uplift at intermediate locations which was captured in the finite-element model as well (Figure 10 (a) – (c)).

The floor diaphragm configuration used tongue-in-groove sheathing panels that prevented lift-off. This was modeled computationally using vertical couplings between the panels. Failure was driven by screw-shear which was captured in the connection UEL models, however since the connection experiments that characterized the UELs did not include fastener tear-out (Figure 10 (g)), this failure mode was beyond the capabilities of the modeling protocol. Peak floor response was characterized by the panels sliding relative to each other which was seen in the computational model as well (Figure 10 (d) – (f)).

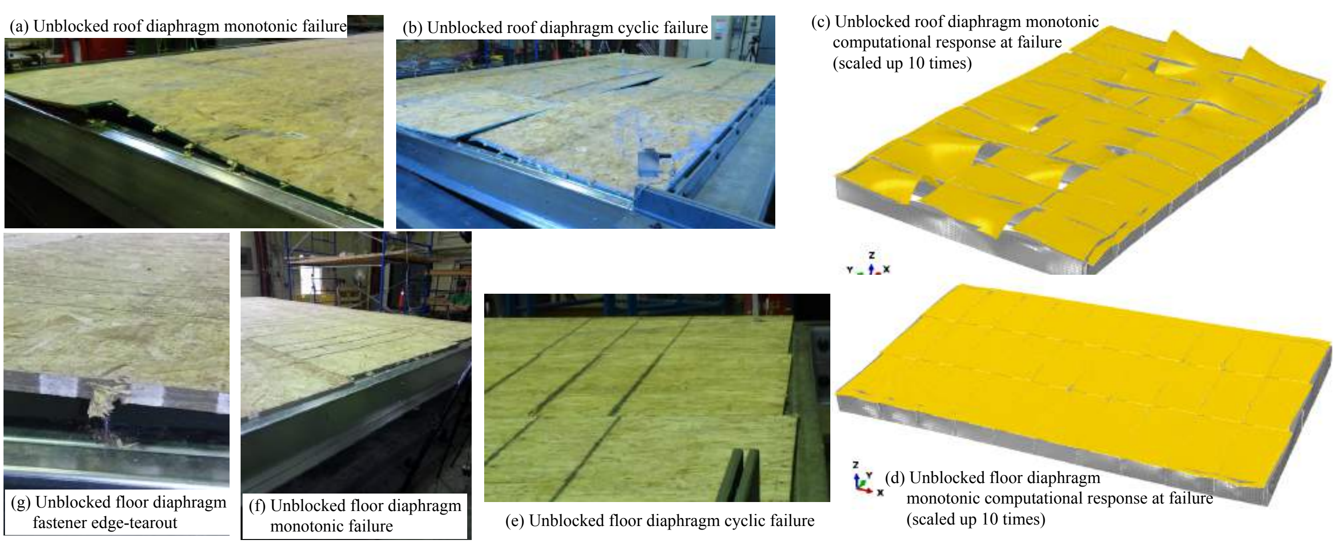

Figure 10 -- Failure modes observed in monotonic and cyclic experiments compared with monotonic computational deformation at failure

Finally, since the computational model includes custom UEL elements that capture pinching response, the cyclic deformation history used in the experimental program was also applied to the model. The panel-to-panel frictional springs described in Section 3.4 do not work under a cyclic loading protocol because the frictional force needs to reverse as soon as unloading initiates, whereas the springs return to their mean position before reversing their internal force. Two sets of analyses were performed for the unblocked roof diaphragm and the floor diaphragm with #10 fasteners, one with full frictional coupling between the panels and the other with no panel friction. The results, plotted in Figure 11, indicated that the full friction and no friction cases bound the actual experimental response, which is closer to the no-friction case for the roof diaphragm due to the lower friction between its panels. As in the monotonic case, the computational models capture the response quite well until peak-load, but fail to converge in the post-peak region as the fasteners reach the steep post-peak softening leg of their backbones.

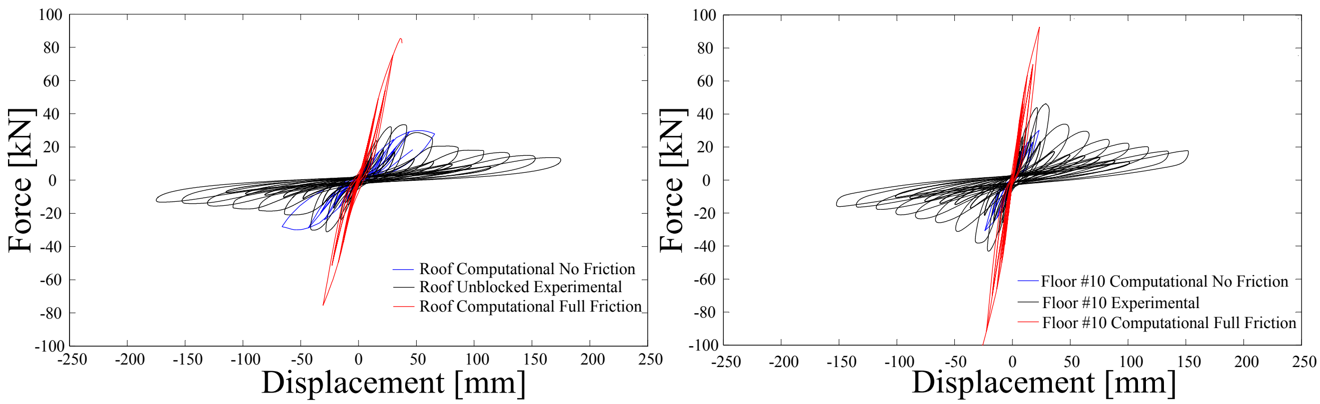

Figure 11 -- Cyclic force-deformation relationships for floor #10 and unblocked roof diaphragms with full friction and no friction modeled between panels

4. Conclusions

This work described results from experimental and computational research conducted on wood-sheathed cold-formed steel floor diaphragms subjected to monotonic and reverse-cyclic loads. The computational model included shell finite-elements, geometric and material non-linearity and panel-to-panel contact. Since the experiments demonstrated that the diaphragm force-deformation behavior and peak capacity were governed by the behavior of the sheathing-to-framing connections, which is consistent with previous research on similar systems, these were characterized carefully using single-fastener cyclic connection tests. The sheathing-to-framing connections were modeled as custom user-defined connection elements with quadri-linear backbones and pinching-type unloading-reloading behavior whose parameters were derived from the connection tests. Furthermore, these elements are also capable of updating their orientations during the analysis.

The computational models captured the peak deformations and loads reached in the monotonic experiments, but experienced convergence difficulties beyond the peak load due to high unloading stiffnesses in the connection backbones. Since these backbones were quadri-linear plots obtained from cyclic connection experiments, the unloading response included a single failing leg with high negative stiffness. The post-peak response for the floor model can potentially be captured by using monotonic experiments to characterize the backbone or by using several more segments in the unloading portion of the response. However, due to the overall brittle nature of the connections, there is no residual capacity or potential for load-redistribution available beyond the peak load, which is why the computationally predicted capacity may safely be considered as the ultimate diaphragm strength. The computational model was also subjected to the reverse-cyclic loading protocol used in the experiment for perfect friction and zero friction cases, and it was observed that these represented upper and lower bounds to the experimental results.

5. Acknowledgements

This material is based upon work supported by the National Science Foundation under Grant Nos. 1301001 (Virginia Tech), 1301033 (University of Massachusetts Amherst) and 1300484 (Johns Hopkins University). Any opinions, findings, and conclusions or recommendations expressed in this material are those of the authors and do not necessarily reflect the views of the National Science Foundation. The first author wishes to thank Virginia Tech researchers Francis Li, Robert Cole and Fannie Tao for helping with the connection experiments, and McGill University researcher Violetta Nikolaidou for providing the diaphragm test data.

6. References

[1] Nikolaidou, V., Latreille, P., Rogers, C.A., and Lignos, D. (2017). Characterization of cold-formed steel framed / wood-sheathed floor and roof diaphragm structures. in *16th World Conference on Earthquake Engineering*. Santiago, Chile.

[2] Nikolaidou, V., Latreille, P., and Rogers, C.A. (2015): Characterization of CFS framed diaphragm behaviour ; Experimental Program Summer 2015. *Research Report prepared for the American Iron and Steel Institute Seismic Code Team, AISI Project Number CM - 432*. Montreal, Canada.

[3] NAHBRC (1999): Innovative Residential Floor Construction: Horizontal Diaphragm Values for Cold Formed Steel Framing.

[4] Peterman, K.D. (2014): Behavior of full-scale cold-formed steel buildings under seismic excitations *Johns Hopkins University*

[5] Dassault-Systems ABAQUS Version 11-2, http://www.3ds.com/products-services/simulia/portfolio/abaqus.

[6] Ding, C. (2015): Monotonic and Cyclic Simulation of Screw-Fastened Connections for Cold-Formed Steel Framing, *Virginia Polytechnic Institute and State University*

[7] SSMA (2013): Product Technical Guide.

[8] Ibarra, L.F., Medina, R.A., and Krawinkler, H. (2005): Hysteretic models that incorporate strength and stiffness deterioration. *Earthquake Engineering and Structural Dynamics*. **34**.

[9] Lowes, L., Mitra, N., and Altoontash, A. (2004): A Beam-Column Joint Model for Simulating the Earthquake Response of Reinforced Concrete Frames. *PEER Report 2003/10*. Berkeley, CA.

[10] McKenna, F., Fenves, G.L., and Scott, M.H. (2000): Open system for earthquake engineering simulation. 2000.

[11] Moen, C.D., Tao, F., and Cole, R. (2016). Monotonic and cyclic backbone response of single shear cold-formed steel screw-fastened connections. in *The International Colloquium on Stability and Ductility of Steel Structures*. Timisoara, Romania.

[12] Peterman, K.D. and Schafer, B.W. (2013): Hysteretic shear response of fasteners connecting sheathing to cold-formed steel studs. *CFS NEES : Advancing Cold-Formed Steel Earthquake Engineering*.

[13] Chatterjee, A., Moen, C.D., Arwade, S.R., and Schafer, B.W. ((in preparation)): Structural Modeling, Response and Reliability of Wood-Sheathed Floor Diaphragms in Cold-Formed Steel Framed Buildings.

[14] Schafer, B.W., Li, Z., and Moen, C.D. (2010): Computational modeling of cold-formed steel. *Thin-Walled Structures*. **48**: 752-762.

[15] Chatterjee, A., Xiang, Y., Moen, C.D., Arwade, S.R., and Schafer, B.W. (2014). Towards Quantifying Beneficial System Effects In Cold-Formed Steel Wood-Sheathed Floor Diaphragms. in *International Specialty Conference on Cold-Formed Steel Structures*. St. Louis, Missouri.

[16] ICC, *International Building Code*. 2012: USA.

[17] Moen, C.D. (2008): Direct Strength Design of Cold-Formed Steel Members with Perforations, *Johns Hopkins University*